https://doi.org/10.5194/angeo-2020-16
Preprint. Discussion started: 13 May 2020

Annales Geophysicae Discussions
Open Access
EGU

Even moderate geomagnetic pulsations can cause fluctuations of foF2 frequency of the auroral ionosphere

Nadezda Yagova[1], Alexander Kozlovsky[2], Evgeny Fedorov[1], and Olga Kozyreva[1]

[1]Schmidt Institute of Physics of the Earth, Moscow,Russia
[2]Sodankylä Geophysical Observatory, Sodankylä, Finland

Correspondence: N. Yagova(nyagova@ifz.ru)

Abstract. Using data of the ionosonde in Sodankylä, (SOD, 67°N, 27°E, Finland), variations of the critical frequency of o-mode radiowave reflected from ionospheric F2 layer (foF2) in $1-5$ mHz frequency range and their possible association with long period (Pc5/Pi3) geomagnetic pulsations are studied. For that, a technique of automatic detection of the foF2 critical frequency from an ionogram is developed and applied to daytime Pc5/Pi3 geomagnetic pulsations and foF2 fluctuations during several months of years 2014-2015 near the maximum of 24-th Solar cycle. The variations of foF2 are compared with the Pc5/Pi3 geomagnetic pulsations at SOD station, and the influence of pulsations' spatial scale is analyzed with the data of a station pair located at the same magnetic meridian but separated in latitude. The variations of foF2 are in the majority of cases decoupled from the geomagnetic pulsations on the ground. Meanwhile, the analysis of geomagnetic and foF2 variations show intervals with noticeable coherence for both horizontal components. These coherent pulsations are predominantly registered in the afternoon sector of the magnetic local time (MLT). Statistically, their spectral content, polarization and spatial distribution differ from averaged parameters of post-noon Pc5 pulsations. The pulsations, coherent to foF2 fluctuations, demonstrate features typical for Alfven field-line resonance. The analysis of space weather conditions favorable for the occurrence of coherent geomagnetic/foF2 pulsations show that these pulsations are registered mostly under moderately disturbed conditions. Comparison of space weather parameters for all the intervals analyzed and the intervals of high geomagnetic/foF2 coherence show that the latter correspond mostly to intermediate values of indexes of geomagnetic (Dst) and auroral (AE) activity, solar wind speed and dynamic pressure fluctuations.

1 Introduction

Modulation of ionospheric parameters by Pc5 pulsations was reported by Pilipenko et al. (2014a, b). Majority of publications are based on the radar observation, i.e. observations of variations of electron concentration at certain altitude in the ionosphere (e.g. Mager et al. (2015); James et al. (2016)). Observations of pulsations in the total electron content (TEC) are rather rare (Pilipenko et al., 2014a, b; Watson et al., 2015; Vorontsova et al., 2016). Watson et al. (2015) reported on TEC variations mea-

https://doi.org/10.5194/angeo-2020-16
Preprint. Discussion started: 13 May 2020

Annales Geophysicae Discussions

sured by GPS at Pc5-6 frequencies. The large-amplitude TEC variations were associated with mainly compressional mode of MHD wave in the magnetosphere. The pulsations were also seen in magnetic field on the ground with two spectral peaks at about 0.9 mHz and 3.3 mHz. The event was observed in the afternoon MLT sector after a steep increase of SW dynamic pressure up to almost 20 nPa. An effect of TEC modulation by ULF wave at low latitudes reported by Vorontsova et al. (2016) is important because the observations were made far away from the resonant L-shells and zones where kinetic modes can occur due to wave-particle interaction. This allows to identify observed pulsations as fast magnetosonic mode.

An intriguing effect of double Pc5 frequency in fluctuations of ionospheric parameters was shown by Kozyreva et al. (2019). However, the effect of ionosphere heating by an intense MHD wave, found by Pilipenko et al. (2014b) at the recovery phase of the magnetic storm is possible only for extremely high Pc5 amplitudes. On the contrary, a role of MHD waves with moderate amplitudes in variations of foF2 critical frequency has not been studied in details.

Our study is aimed on variations of foF2 critical frequency at Pc5/Pi3 frequencies and geomagnetic pulsations in the same frequency range, both for individual events and statistically.

2 Data of observations and their processing

2.1 Data

The Sodankylä Geophysical Observatory (SOD) ionosonde is located at geographic coordinates 67.3 N, 26.7 E. It makes an ionogram once a minute. A detailed description of the ionosond observations can be found in (Kozlovsky et al., 2013). SOD magnetometer is a part of IMAGE magnetometer network (Taskanen, 2009), and three components of the geomagnetic field are available with 10 s sampling rate. For the analysis of Pc5 spatial distribution, and we also use the data of the MAS station, which is a part of IMAGE. Station information is summarized in Table 1.

To analyzed space weather conditions, OMNI data including interplanetary magnetic field, solar wind speed and dynamic pressure, re-calculated to the sub-solar point of the magnetosphere (Bargatze et al., 2005), are used, and also Dst and AE indexes are used. The data are available at http://cdaweb.gsfc.nasa.gov

We use for the analysis the interval from April of 2014 till the end of 2015 (totally 21 months), and take daytime intervals when foF2 critical frequency was seen with quality and time resolution enough for spectral analysis. A summary of intervals analyzed is given in Table 2.

2.2 foF2 automatic detection from ionograms

Although visual detection of a critical frequency from an ionogram with clearly expressed layers is not difficult, an automatic detection method is necessary for an analysis of high frequency variations of critical frequencies. The difficulties of this procedure are caused by different intensity of the reflected signal, different contrast between reflection maximum and the background, occurrence of sporadic layers, man-made interference, etc. Because of these reasons, routine techniques of automatic foF2 detection can become unstable, even when visual detection is possible.

https://doi.org/10.5194/angeo-2020-16
Preprint. Discussion started: 13 May 2020


Annales Geophysicae Discussions

Below, we present a method based on the approximation of the reflection boundary in a wide range of altitudes to suppress the influence of local gaps and peaks in reflection.

The highest frequency reflection boundary in such a presentation is characterized by almost linear growth of frequency at low altitudes, then growth becomes slower, and finally it saturates at the critical frequency. We approximate this dependence by a Lorentsian type function

$$f(h) = f_1 + \Delta f \frac{k(\frac{h}{h_1} - 1)^\alpha}{k(\frac{h}{h_1} - 1)^\alpha + 1} \tag{1}$$

Starting altitude is taken at $h_1 = 235$ km Coefficients f_1, $\Delta f = f_2 - f_1$, k, and α are found as a result of fitting procedure, described below. The boundary is determined as a line where the following two conditions are fulfilled:

- Signal intensity I at the boundary should be high
- Amplitude ratio R of the signal intensity at the boundary line to the power above it should also be high

As four fitting factors are used, a 9-point iteration procedure is organized and a parameter K_t, determined as $K_t^2 = cI^2 + (1-c)R^2$ is maximized over the "cross" in space of parameters $K_t(x_0, x_0 - \Delta x_i, x_0 + \Delta x_i)$, where x is a point in the space of parameters, and i is a parameter number. The initial approximation is taken from the database created manually for several typical types of $f(h)$ dependence. foF2 is then determined as a value of (1) in the altitude region with weak dependence $f(h)$. The other requirement is a continuity of time dependence $f(t)$. The threshold value for the time derivative of foF2 is estimated from the variance of an interval of length t_1. For $t > t_1$, the set of parameters calculated at the previous step is taken as the initial approximation. If an iteration procedure gives a value of foF2 with the difference from the previous values exceeding the threshold value, the other initial approximation from the database is taken, and the procedure is repeated. If all the initial approximations give a value, outstanding far from the previous ones, this point is excluded, and the iteration procedure is started from the next time instant. Examples of approximation curves are given in Figure 1 for 3 ionograms, registered on 24 October (day 297) 2014. The continuity condition allows to suppress the influence of additional reflection maxima and bifurcations. The list of the days and time intervals selected with the automatic detection procedure and tested visually for each tenth point, ASCII files and pictures of foF2 time variations for the selected intervals are available in supplementary files. The selected intervals form the database for the analysis.

An example of diurnal variations of critical frequency obtained with the technique described is given in Figure 2 for the 3 January (day 003) 2015. Note, that the ionograms are rotated by 90° in respect to usual $f - H$ presentation.

A collection of all the reconstructed foF2 can be found in supplementary files.

2.3 Pre-processing, statistical and spectral analysis

Two horizontal components are analyzed for magnetic field recordings. We use the notation b for the magnetic field of pulsation to discriminate it from the main magnetic field B. We denote pulsations of foF2 as ΔfoF2.

https://doi.org/10.5194/angeo-2020-16
Preprint. Discussion started: 13 May 2020


Annales Geophysicae Discussions

Statistical analysis includes distribution over MLT, parameters of pulsations and the space weather during the interval analyzed and preceding it. We studied Dst and AE geomagnetic indexes, vertical component of the interplanetary magnetic field IMF B_Z, solar wind velocity V and dynamic pressure P_{sw} and the maximal amplitude of P_{sw} fluctuations.

The method, described in the previous section, allows to get foF2 with the time resolution, enough for spectral estimates and comparison with the geomagnetic pulsations based on cross-spectral analysis. For that, power spectral density (PSD) is estimated with a Blackman-Tukey method (Kay, 1988) in a sliding 64 points window with 5 min shift between adjacent intervals. Cross-spectra are calculated for foF2 variations, on one hand, and components of the geomagnetic field pulsations, on the other hand. For the intervals with high spectral coherence γ^2, phase difference $\Delta\varphi$ is estimated.

3 Results

3.1 foF2 variations and geomagnetic pulsations at SOD

3.1.1 Examples

We present two examples of foF2 and geomagnetic variations simultaneously recorded at SOD. Variations of geomagnetic field components and foF2 at SOD on 11 March (Day 70) 2015 (event 1) are presented in Figure 3. Peak-to-peak amplitudes of geomagnetic field and foF2 are about 10 nT and 0.08 MHz, respectively. PSD spectra for both geomagnetic and foF2 variations, spectral coherence and phase difference are presented in Figure 4. The normalized PSD spectrum of geomagnetic pulsations has two broad maxima at $f_1 = 2.3$ and $f_2 = 3.2$ mHz. The spectrum of foF2 variations has a maximum at a frequency $f = 3.8$ mHz. Spectral coherence is high ($\gamma^2 > 0.75$) at low frequency part of spectrum $f < 2$ mHz, and a minor coherence peak with maximal $\gamma^2 = 0.6$ is found near the f_2 frequency.

Figure 5 illustrates the space weather conditions for event 1. The start point of the interval is taken as zero of time axis τ at panels (a-e) of Figure 5. It is seen from the Figure, that geomagnetic conditions were quiet and no magnetic storms occurred during at least four days before the event, Dst> -20 nT (Figure 5a). However, the auroral activity was essential and maximal AE reached 500 nT (Figure 5b). This activation followed the interval of negative B_Z with variations of almost 20 nT amplitude (Figure 5d). For this event, SW speed V was about 400 km/s (Figure 5c), SW dynamic pressure $P_{sw} \approx 4$ nPa (Figure 5e). P_{sw} fluctuations are shown in more details in Figure 5f. Their amplitude was about 0.7 nPa and their apparent period was about 5 minutes. This corresponds to frequency $f = 3.3$ mHz, i.e. it approximately agrees with the f_2 frequency of pulsations at SOD.

The results for the pulsations recorded on 11 July (Day 192) 2015 (event 2) are presented in Figures 6 and 7, which have the same format, as Figures 3 and 4. Peak-to-peak amplitudes of the geomagnetic and foF2 pulsations are about 80 nT and 0.08 MHz, respectively. A clear maximum at $f_1 \approx 2.5$ mHz is seen in both geomagnetic and foF2 PSD spectra (Figure 7a). At the second frequency $f_2 \approx 3.5$ mHz a maximum is seen only in foF2 variations, while in the geomagnetic pulsations this frequency is marked only as a plateau in the PSD spectrum. However, both spectral maxima are seen clearly in the coherence spectrum (Figure 7b), and the phase difference is different for these two frequencies (Figure 7c).

https://doi.org/10.5194/angeo-2020-16
Preprint. Discussion started: 13 May 2020

Annales Geophysicae Discussions

Space weather conditions for this event are summarized in Figure 8, which has the same format as Figure 5. No geomagnetic storms were registered during last 4 days before this event, as Dst exceeds $= -30$ nT throughout the interval (Figure 8a). Meanwhile, auroral activity is high: two auroral activations are seen at $\tau = -8$ and -4 hours with maximal AE$= 1300$ nT and (700 nT), respectively (Figure 8b). The first activation developed after 2 hour interval of negative B_z, while the second one corresponds to B_z turn from -10 to almost $+15$ nT (Figure 8d). For this event, V is about 600 km/s (Figure 8c), maximal P_{sw} was ≈ 9 nPa and then dropped to 5 nPa and slowly decrease to about 3 nPa (Figure 8e). Amplitude of P_{sw} fluctuations during the 45 minute interval shown in Figure 8f was about 0.5 nPa and their apparent period was about $4-5$ minutes. The main frequency of P_{sw} pulsations is 3.7 mHz, i.e. it approximately corresponds to f_2 frequency in foF2 variations, registered at SOD.

3.1.2 Statistics

A MLT distribution of occurrence of the foF2 variations is shown in Figure 9. One can see from the Figure, that Pc5/Pi3 variations of foF2 are predominantly registered in the post-noon MLT sector with maximal probability at MLT 12-15.

Figure 10a shows frequency distributions of geomagnetic and foF2 pulsations at SOD. f_1 is a frequency of the first spectral maximum in the range from 1.5 to 5.5 mHz. The frequency distribution of foF2 fluctuations is enriched with frequencies ($f_1 > 3.7$ mHz) in comparison with the distribution of the geomagnetic pulsations. The distribution of Pc5/Pi3 intervals over $foF2-b$ spectral coherence at SOD are shown in Figure 10b for two horizontal components. For both components, spectral coherence $\gamma^2 < 0.375$ dominates. The fraction of $\gamma^2 \geq 0.375$ intervals is $1/6$ and $1/8$ for b_X and b_Y components, respectively, the fraction of $\gamma^2 \geq 0.5$ is less than 3% for both components.

This means, that in majority cases, Pc5/Pi3 geomagnetic pulsations and variations of foF2 critical frequency at the same point are decoupled. This effect can be seen from both different spectral content and low spectral coherence of magnetic and foF2 fluctuations.

However, the coherent foF2 and geomagnetic pulsations do exist, and a question arises about the pulsation properties and external parameters, favorable for their occurrence. To answer this question, the geomagnetic pulsations at SOD for which $b_X - foF2$ coherence is high ($\gamma^2 > 0.5$) are compared with all the intervals, selected for spectral analysis of foF2 fluctuations at SOD (Table 2).

To avoid the influence of difference in seasonal and diurnal variations between the selected pulsations and average pulsation properties, the statistics for all the pulsations is calculated with the weight functions, which are found from the seasonal and diurnal variations of coherent pulsations. Figure 11 illustrates the difference between coherent and pulsations and averaged properties of all pulsations for three parameters: PSD_{bx} (Figure 11a), PSD ratio $R_{XY} = PSD_{bx}/PSD_{by}$ (Figure 11b), and the b_X PSD ratio along a magnetic meridian $R_\Phi = PSD_{bx}(\Phi)/PSD_{bx}(\Phi + \Delta\Phi)$ (Figure 11c). The latter is calculated for SOD-MAS station pair (MAS station is located nearly at the same magnetic meridian, but 2° northward). PSD_{bx} for coherent pulsations is enriched with frequencies $f > 2$ mHz in comparison with the background pulsations. In this frequency band, R_{XY} also increases and R_Φ demonstrates a non-monotonous dependence on frequency with minimum at $f = 2.7$ mHz and growth at $f \geq 3$ mHz. These features are only weakly seen in averaged $R_\Phi(f)$ dependence for all pulsation intervals.

https://doi.org/10.5194/angeo-2020-16
Preprint. Discussion started: 13 May 2020

Annales Geophysicae Discussions

To understand, what space weather conditions are favorable for generation of coherent $b_X - foF2$ pulsations, we compare the geomagnetic indexes and SW/IMF conditions for intervals when coherent $b_X - foF2$ were registered with all the intervals analyzed. The influence of seasonal and diurnal variation was eliminated in the same manner, as for pulsation parameters. We use for the analysis the 4-day minimum Dst and 6-hour maximal AE, as Pc5 amplitudes are maximal at recovery phase of geomagnetic storms (Posch et al., 2003), and auroral substorms are followed by Pi3 pulsations (Kleimenova et al., 2002) and Pc5 waves with high azimuthal and intermediate wavenumbers (Zolotukhina et al., 2008; Mager et al., 2019). The results for Dst and AE indexes are summarized in Figure 12. Coherent pulsations tend to occur under moderate geomagnetic and auroral activity. The most favorable Dst interval is from -100 to -50 nT (Figure 12a), and for AE index it is from 250 to 500 nT (Figure 12b). Actually, the selection procedure, used in the present study to detect intervals with clearly seen foF2 fluctuations, is limited by quiet and moderately disturbed geomagnetic conditions. This leads to low probabilities to detect foF2 fluctuations at Pc5/Pi3 frequencies under highly disturbed conditions. This naturally follows from the condition of existence of clear F2 trace at an ionogram, which is, necessary for the foF2 pulsation detection procedure. During geomagnetic storms detection of the foF2 variations is often impossible because of enhanced ionization in the lower ionospheric layers (E and/or D).

Occurrence and parameters of high-latitude Pc5s are controlled by interplanetary parameters, especially IMF B_Z component, variations of solar wind dynamic pressure P, and solar wind velocity V (Baker et al., 2003). Distributions of these three parameters are presented in Figure 13. We have taken 3-hour mean values of B_Z and V and 3-hour maximal value of ΔP_{sw}. Figure 13a shows that coherent events tend to occur during positive B_Z intervals. This result agrees with moderate geomagnetic and auroral activity, favorable for coherent foF2-b pulsations. Figures 13 (b) and (c) show that selected coherent events tended to occur during somewhat higher SW speed and higher amplitudes of SW pressure fluctuations, than it is found for all the intervals.

4 Discussion and conclusion

The presented study of day-time fluctuations of foF2 in $1-5$ mHz frequency range has been undertaken for quiet and moderately disturbed geomagnetic conditions when foF2 frequency can be unambiguously revealed from ionograms. For that, a technique of automatic detection of foF2 from ionogram was developed and verified by visual inspection.

Our analysis of correspondence between Pc5/Pi3 and foF2 variations at SOD showed that relatively rare cases of coherent variations occur preferably in the afternoon MLT sector under moderately disturbed geomagnetic conditions. As a rule, post-noon Pc5 are characterized by higher azimuthal wave-numbers than morningside Pc5s (see Min et al. (2017) and references therein). They are often associated with kinetic modes originated from wave-particle interactions (see e.g. Mager et al. (2013) and references therein). For these waves, the amplitudes on the ground are strongly attenuated by the ionosphere (Kokubun et al., 1989), while their amplitudes in the magnetosphere both in the magnetic field and in particle flux can be high (Baddeley et al., 2004).

https://doi.org/10.5194/angeo-2020-16
Preprint. Discussion started: 13 May 2020

Amplitude of SW dynamic pressure fluctuations show an association with occurrence of coherent $foF2-B$ pulsations, as well as the observed periods are close in the individual cases (Figures 5, 8). This effect is in favor of global character of the observed coherent pulsations (Kepko et al., 2002; Yagova et al., 2007; Viall et al., 2009).

On the other hand, for the intervals, when ground Pc5s are coherent with foF2 variations, the magnetic pulsations show typical features of the Alfven field-line resonance in spectral content, polarization, and amplitude distribution along the meridian (Baransky et al., 1995) in coherent $foF2-B_X$ pulsations in comparison with typical afternoon Pc5s at SOD.

A similar result follows from the comprehensive statistical analysis of correspondence between geomagnetic and Cosmic Noise Adsorbtion (CNA) pulsations (Spanswick et al., 2005), who found that geomagnetic pulsations with FLR features demonstrate a better correspondence with CNA pulsations than non-FLR Pc5s.

However, physical reasons for our and (Spanswick et al., 2005) results may be different, because of different particle energies and Pc5 types. A detailed case study of magnetic field and electron flux pulsations at four Cluster satellites located at different L-shells in the magnetosphere and geomagnetic and CNA pulsations on the ground (Motoba et al., 2013) showed rather complicated space distribution and time variation of geomagnetic and electron pulsations and their inter-relation. The picture changed dramatically within 30-40 minutes, and the pulsation in space was, probably, a mix of compressional and Alfven modes. The authors found that the amplitude of compressional mode was critical for effective modulation of electron flux, but the contribution of shear Alfven resonance was also non-negligible.

For the first time, a statistical study of foF2 variations in Pc5/Pi3 range and their relation to geomagnetic pulsation in the conjugated position at SOD station and its spatial distribution along a magnetic meridian. It is shown that not only storm-time Pc5s can modulate the ionosphere foF2, but also non-storm pulsations with moderate amplitudes. It is important, because in such conditions, F2 layer is not blanketed by lower layers.

Sample availability. All the intervals used in the analysis are visually checked (for each 10-th point) and presented in the table file. The foF2 values, obtained with Eq.(1) for all the intervals analyzed, are available both as jpeg figures and ASCII files. A file name has a structure SOD-YYYY-DDD-foF2, where YYYY is a year and DDD is a day number. Each ASCII file contains two columns:

1. time (seconds) from 00:00 UT
2. foF2 (MHz).

Author contributions. N. Yagova: the approximation algorithm, cross-spectral and statistical analysis; A. Kozlovsky: pre-processing and visual check of ionosonde data; E. Fedorov: interpretation of results, analysis of wave parameters; O. Kozyreva: selection of events, algorithms and codes for visualization; all the authors: MS preparation

Competing interests. The authors have no competing interests

https://doi.org/10.5194/angeo-2020-16
Preprint. Discussion started: 13 May 2020

Annales Geophysicae Discussions
Open Access
EGU

Acknowledgements. We thank SGO (http://www.sgo.fi/) for SOD magnetometer and ionosonde data, Finnish Meteorological Institute for MAS magnetometer data, CDAWEB (https://cdaweb.gsfc.nasa.gov) for OMNI data, and World data center Kyoto (http://wdc.kugi.kyoto-u.ac.jp/index.html) for AE and Dst indexes. The study was supported by the Academy of Finland grants 298578 and 310348 and RFBR grant 20-05-00787 (OK) and state contract with IPE (NY, EF). Useful discussions with V.A. Pilipenko are appreciated.

https://doi.org/10.5194/angeo-2020-16
Preprint. Discussion started: 13 May 2020

References

Baddeley, L. J., Yeoman, T. K., Wright, D. M., Trattner, K. J., and Kellet, B. J.: A statistical study of unstable particle populations in the global ringcurrent and their relation to the generation of high m ULF waves, Ann. Geophys., 22, 4229–4241, https://doi.org/10.5194/angeo-22-4229-2004, 2004.

Baker, G., Donovan, E. F., and Jackel, B. J., A comprehensive survey of auroral latitude Pc5 pulsation characteristics, J. Geophys. Res., 108, 1384, doi:10.1029/2002JA009801, 2003.

Baransky, L. N., Fedorov, E. N., Kurneva, N. A., Pilipenko, V. A., Green, A. W. , and Worthington, E. W.: Gradient and polarization methods of the ground-based hydromagnetic monitoring of magnetospheric plasma, J. Geomagn. Geolect., 47, 1293-1309, 1995.

Bargatze, L.F., R.L. McPherron, J. Minamora and D.Weimer, A new interpretation of Weimer et al's solar wind propagation delay technique, J. Geophys. Res., 110, A07105, doi:10.1029/2004JA010902, 2005.

James, T. K., Yeoman, M. K., Mager, P. N., and Klimushkin, D. Y.: Multiradar observations of substorm-driven ULF waves, J. Geophys. Res. Space Physics, 121, 5213-5232, doi:10.1002/2015JA022102, 2016.

Kay, S. M.: Modern spectral estimation: Theory and application, Prentice-Hall, Prentice Hall, New Jersey, USA 543 pp., 1988.

Kleimenova, N. G., Kozyreva, O. V., Kauristie, K., Manninen, J., and Ranta, A.: Case studies on the dynamics of Pi3 geomagnetic and riometer pulsations during auroral activations, Ann. Geophys., 20, 151-159, https://doi.org/10.5194/angeo-20-151-2002, 2002.

Kepko, L., Spence, H. E., and Singer, H. J.: ULF waves in the solar wind as direct drivers of magnetospheric pulsations, Geophys. Res. Lett., 29, 1197, https://doi.org/10.1029/2001GL014405, 2002.

Kokubun, S., Erickson, K. N., Fritz, T. A., and McPherron, R. L.: Local time asymmetry of Pc 4-5 pulsations and associated particle modulations at synchronous orbit, J. Geophys. Res., 94(A6), 6607-6625, doi:10.1029/JA094iA06p06607, 1989.

Kozlovsky, A., Turunen, T., and Ulich, T.: Rapid-run ionosonde observations of traveling ionospheric disturbances in the auroral ionosphere, J. Geophys. Res. Space Physics, 118, 5265- 5276, doi:10.1002/jgra.50474, 2013.

Kozyreva, O. , Kozlovsky, A. , Pilipenko, V., Yagova, N.: Ionospheric and geomagnetic Pc5 oscillations as observed by the ionosonde and magnetometer at Sodankylä, Advances in Space Research, 63, 2052-2065, https://doi.org/10.1016/j.asr.2018.12.004, 2019.

Mager, P. N., Klimushkin, D. Yu., and Kostarev, D. V. (2013), Drift-compressional modes generated by inverted plasma distributions in the magnetosphere, J. Geophys. Res. Space Physics, 118, 4915–4923, doi:10.1002/jgra.50471.

Mager, P. N., Berngardt, O. I., Klimushkin, D. Yu., Zolotukhina, N. A., Mager, O. V.: First results of the high-resolution multibeam ULF wave experiment at the Ekaterinburg SuperDARN radar: ionospheric signatures of coupled poloidal Alfven and drift-compressional modes. J. Atmos. Solar-Terr. Phys. 130-131, 112-126, 2015.

Mager, O. V., Chelpanov, M. A., Mager, P. N., Klimushkin, D. Y., Berngardt, O. I.: Conjugate ionosphere-magnetosphere observations of a sub-Alfvenic compressional intermediate-m wave: A case study using EKB radar and Van Allen Probes. Journal of Geophysical Research: Space Physics, 124, 3276-3290. https://doi.org/10.1029/2019JA026541, 2019.

Min, K., Takahashi, K., Ukhorskiy, A. Y., Manweiler, J. W., Spence, H. E., Singer, H. J., Claudepierre, S. G., Larsen, B. A., Soto-Chavez, A. R., and Cohen, R. J. (2017), Second harmonic poloidal waves observed by Van Allen Probes in the dusk-midnight sector, J. Geophys. Res. Space Physics, 122, 3013–3039, doi:10.1002/2016JA023770.

Motoba, T., Takahashi, K. , Gjerloev, J., Ohtani, S. and Milling, D. K.: The role of compressional Pc5 pulsations in modulating precipitation of energetic electrons, J. Geophys. Res. Space Physics, 118, 7728-7739, doi:10.1002/2013JA018912, 2013.

https://doi.org/10.5194/angeo-2020-16
Preprint. Discussion started: 13 May 2020

Pilipenko, V., Belakhovsky, V. , Kozlovsky, A. , Fedorov, E. , and Kauristie, K.: ULF wave modulation of the ionospheric parameters: Radar and magnetometer observations, J. Atmos. Sol. Terr. Phys., 108, 68-76, doi:10.1016/j.jastp.2013.12.015, 2014.

Pilipenko, V., Belakhovsky, V. , Murr,D. , Fedorov, E. , and Engebretson M.: Modulation of total electron content by ULF Pc5 waves, J. Geophys. Res. SpacePhysics,119,4358-4369, doi:10.1002/2013JA019594, 2014.

Posch, J. L., Engebretson, M. J., Pilipenko, V. A., Hughes, W. J., Russell, C. T., and Lanzerotti, L. J.: Characterizing the long-period ULF response to magnetic storms, J. Geophys. Res., 108, 1029, doi:10.1029/2002JA009386, A1, 2003.

Spanswick, E., Donovan, E. , and Baker, G.: Pc5 modulation of high energy electron precipitation: Particle interaction regions and scattering efficiency, Ann. Geophys., 23, 1533-1542, 2005.

Tanskanen, E. I.: A comprehensive high-throughput analysis of substorms observed by IMAGE magnetometer network: Years 1993-2003 examined, J. Geophys. Res., 114, A05204, doi:10.1029/2008JA013682, 2009.

Viall, N. M., Kepko, L., and Spence, H. E. (2009), Relative occurrence rates and connection of discrete frequency oscillations in the solar wind density and dayside magnetosphere, J. Geophys. Res., 114, A01201, doi:10.1029/2008JA013334.

Vorontsova, E., Pilipenko, V., Fedorov, E., Sinha, A.K., Vichare, G.: Modulation of total electron content by global Pc5 waves at low latitudes, Adv. Space Res., 57, 309–319, doi: 10.1016/j.asr.2015.10.041, 2016.

Watson, C., Jayachandran, P. T., Singer, H. J., Redmon, R. J., and Danskin, D.: Large-amplitude GPS TEC variations associated with Pc5-6 magnetic field variations observed on the ground and at geosynchronous orbit, J. Geophys. Res. Space Physics, 120, 7798- 7821, doi:10.1002/2015JA021517, 2015.

Yagova N., V. Pilipenko, J. Watermann, K. Yumoto: Control of high latitude geomagnetic fluctuations by interplanetary parameters: The role of suprathermal ions, Annales Geophysicae, 25, N4, 1037-1047, 2007.

Zolotukhina, N. A., Mager, P. N., and Klimushkin, D. Yu.: Pc5 waves generated by substorm injection: a case study, Ann. Geophys., 26, 2053-2059, https://doi.org/10.5194/angeo-26-2053-2008, 2008.

https://doi.org/10.5194/angeo-2020-16
Preprint. Discussion started: 13 May 2020

Annales Geophysicae Discussions
Open Access
EGU

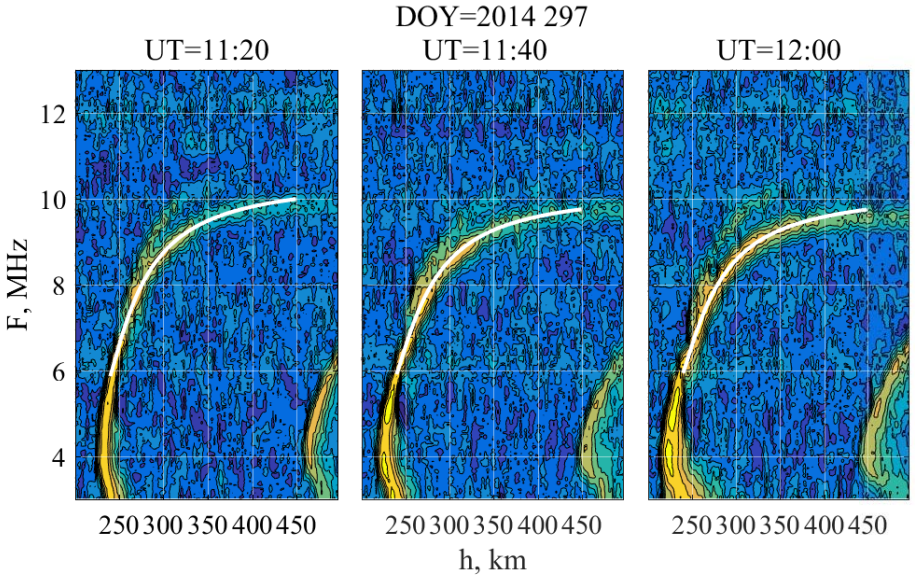

Figure 1. Examples of approximations of F(h) dependence with eq. (1)

https://doi.org/10.5194/angeo-2020-16
Preprint. Discussion started: 13 May 2020

Annales Geophysicae Discussions
Open Access
EGU

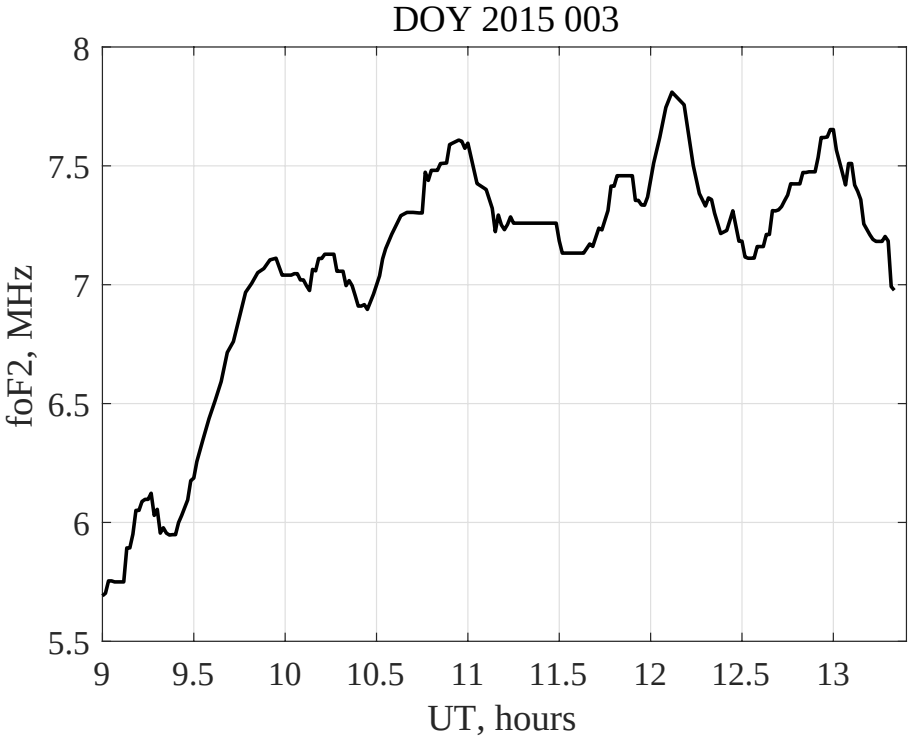

Figure 2. Variation of foF2 frequency during 4.5 hours on day 2015 003 , obtained with eq. (1)

https://doi.org/10.5194/angeo-2020-16
Preprint. Discussion started: 13 May 2020

Annales Geophysicae Discussions
Open Access
EGU

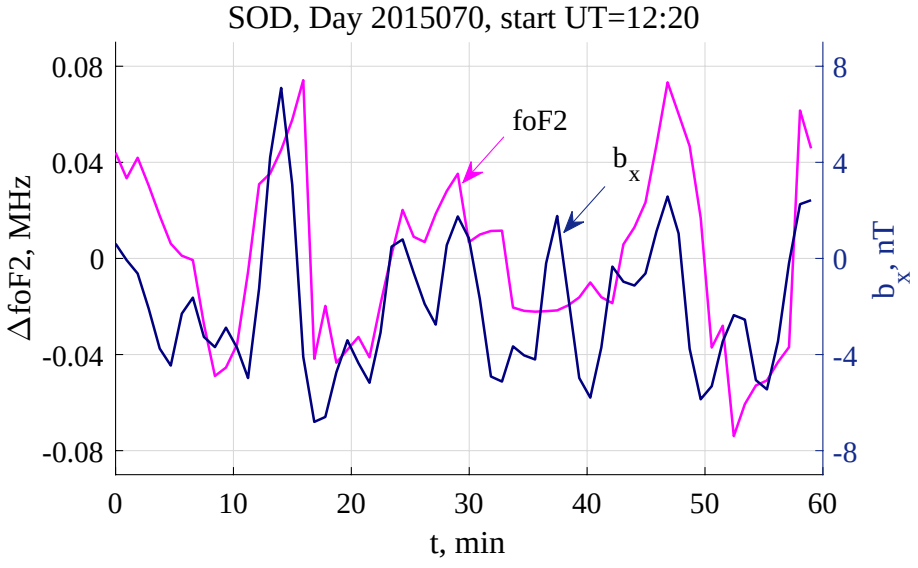

Figure 3. Variation of foF2 and geomagnetic pulsations at SOD during event 1

https://doi.org/10.5194/angeo-2020-16
Preprint. Discussion started: 13 May 2020

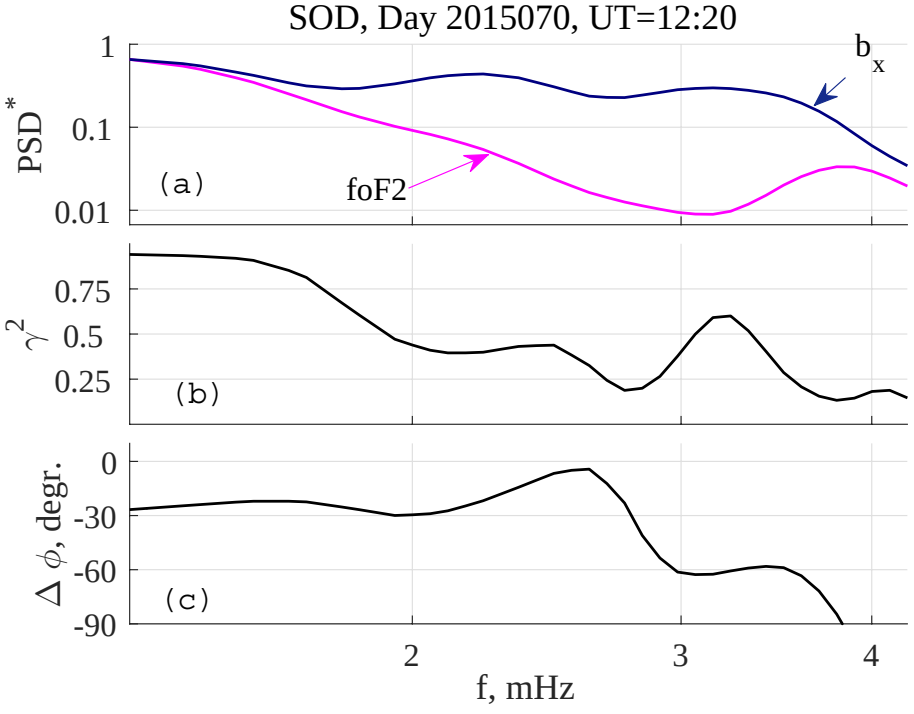

Figure 4. Spectral parameters for the event 1: (a) normalized PSD spectra of foF2 and b_X pulsations, (b) spectral coherence between foF2 and b_X; (c) phase difference

https://doi.org/10.5194/angeo-2020-16
Preprint. Discussion started: 13 May 2020

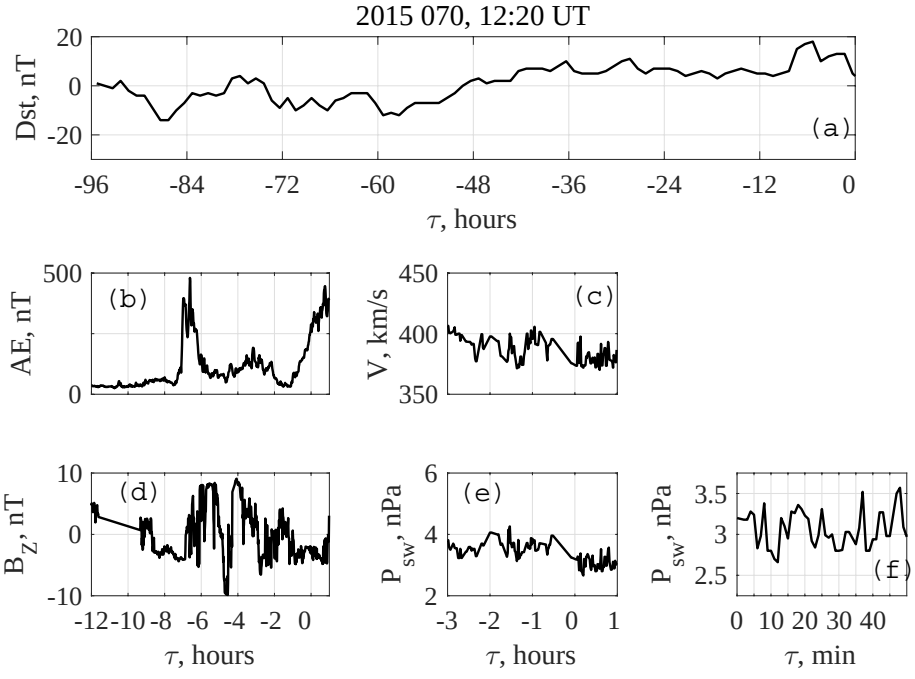

Figure 5. Space weather conditions for the event 1. (a) Dst index during last four days; (b) AE index during the interval and 12 hours before; (c) SW speed during the interval and 3 hours before; (d) IMF B_Z during the interval and 12 hours before; (e) SW dynamic pressure during the interval and 3 hours before; (f) details of SW dynamic pressure fluctuations during the interval.

https://doi.org/10.5194/angeo-2020-16
Preprint. Discussion started: 13 May 2020

Annales Geophysicae Discussions
Open Access
EGU

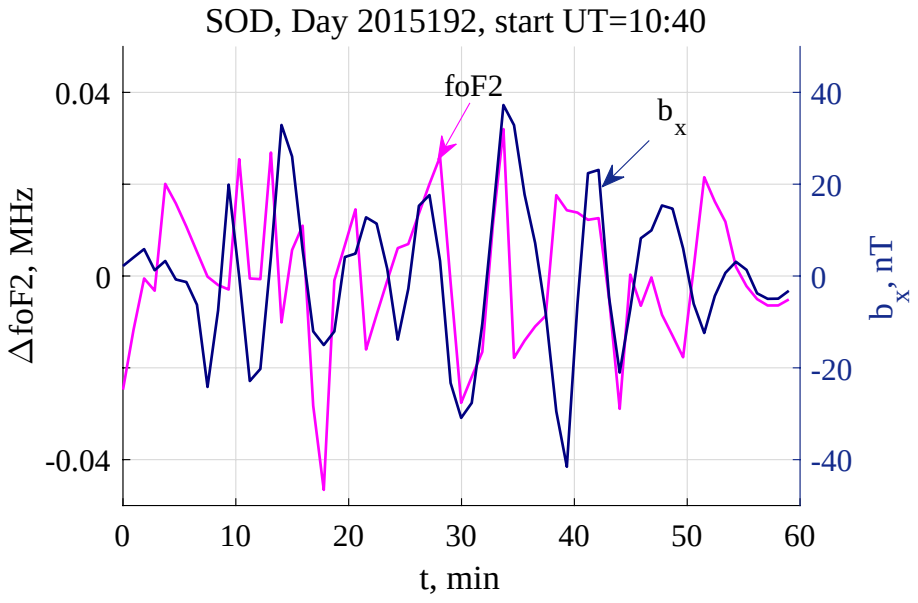

Figure 6. Variation of foF2 and geomagnetic pulsations at SOD during event 2

https://doi.org/10.5194/angeo-2020-16
Preprint. Discussion started: 13 May 2020

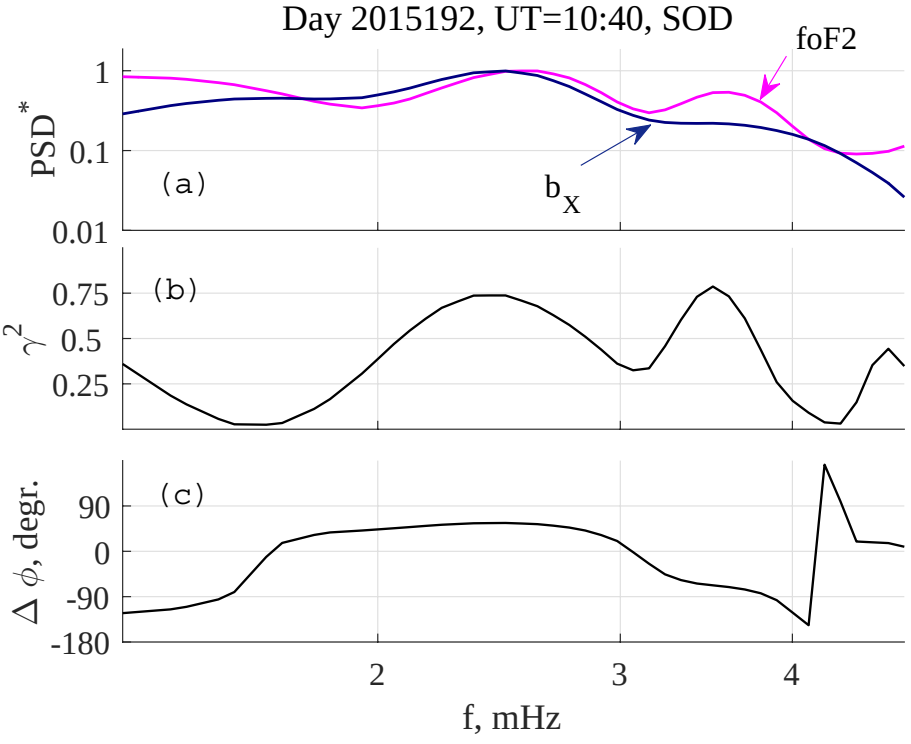

Figure 7. Spectral parameters for the event 2: (a) normalized PSD spectra of foF2 and b_X pulsations, (b) spectral coherence between foF2 and b_X; (c) phase difference.

https://doi.org/10.5194/angeo-2020-16
Preprint. Discussion started: 13 May 2020

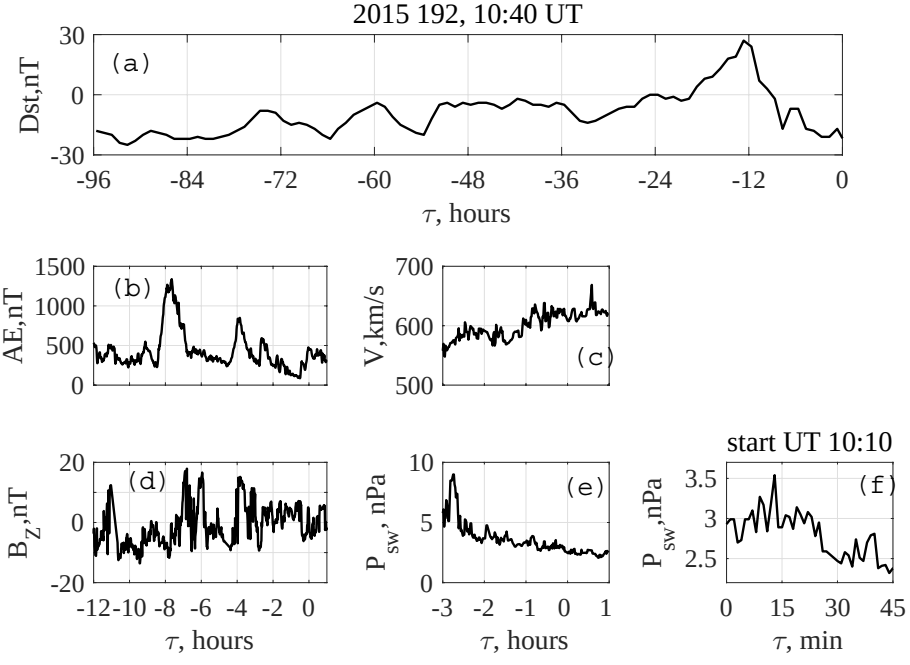

Figure 8. Space weather conditions for the event 2. (a) Dst index during last four days; (b) AE index during the interval and 12 hours before; (c) SW speed during the interval and 3 hours before; (d) IMF B_Z during the interval and 12 hours before; (e) SW dynamic pressure during the interval and 3 hours before; (f) details of SW dynamic pressure fluctuations during the last hour before the interval.

https://doi.org/10.5194/angeo-2020-16
Preprint. Discussion started: 13 May 2020

Annales Geophysicae Discussions
Open Access
EGU

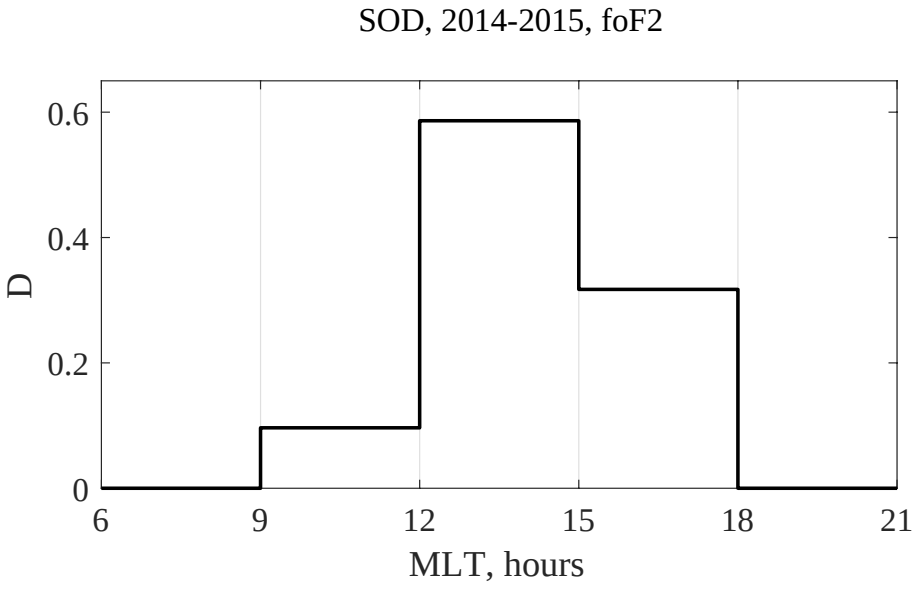

Figure 9. Averaged MLT distribution of occurrence of foF2 fluctuations in $1-5$ mHz frequency band.

https://doi.org/10.5194/angeo-2020-16
Preprint. Discussion started: 13 May 2020

Annales Geophysicae Discussions
Open Access
EGU

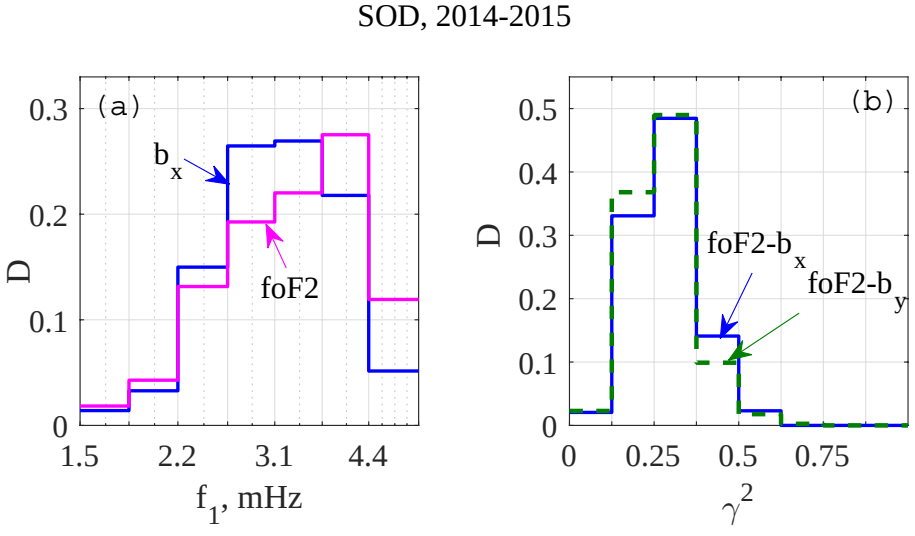

Figure 10. Averaged distributions of parameters of foF2 fluctuations and Pc5/Pi3 pulsations at SOD: (a) frequency of the first spectral maximum of b_X (blue) and foF2 (magenta); (b) spectral coherence of foF2-b_X (blue) and foF2-b_Y (green).

https://doi.org/10.5194/angeo-2020-16
Preprint. Discussion started: 13 May 2020

Annales Geophysicae Discussions
Open Access
EGU

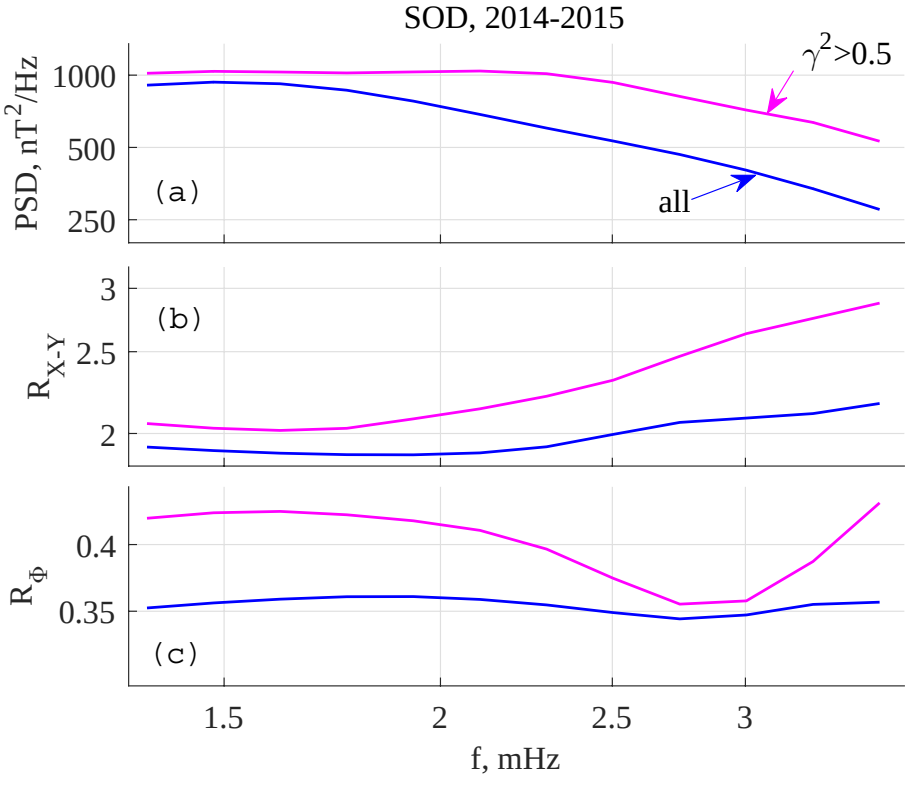

Figure 11. Comparison of averaged parameters of coherent with foF2 (magenta) and all intervals analyzed (blue) Pc5/Pi3 pulsations at SOD: (a) PSD; (b) $R_{X-Y} = PSD_{bx}/PSD_{by}$ spectral ratio; (c) $R_{\Phi} = PSD_{bx}$(SOD)/PSD_{bx}(MAS) spectral ratio.

https://doi.org/10.5194/angeo-2020-16
Preprint. Discussion started: 13 May 2020

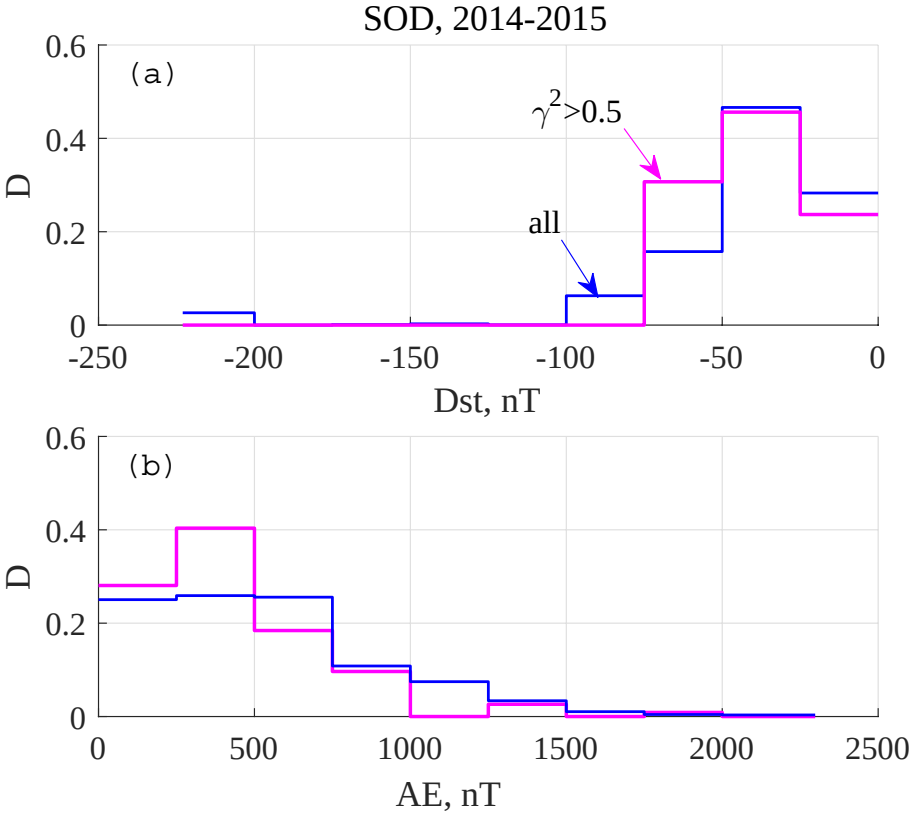

Figure 12. Comparison of geomagnetic indexes for coherent foF2-*b* (magenta) and all intervals analyzed (blue) Pc5/Pi3 pulsations at SOD: (a) distribution over Dst index; (b) distribution over AE index.

https://doi.org/10.5194/angeo-2020-16
Preprint. Discussion started: 13 May 2020

Annales Geophysicae Discussions
Open Access
EGU

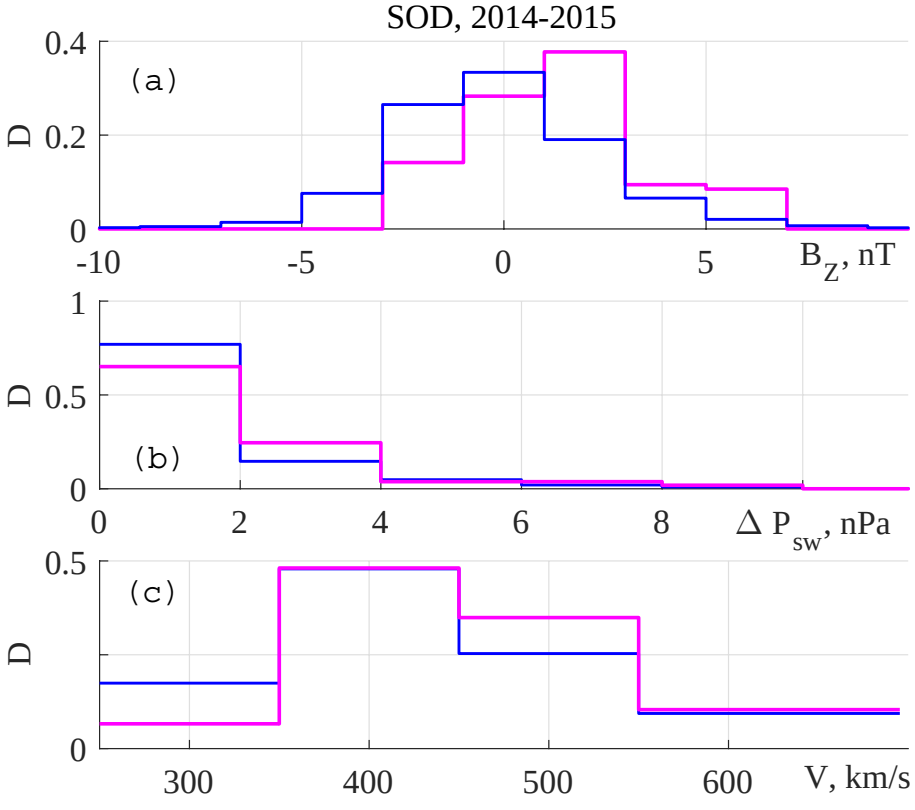

Figure 13. Comparison of SW/IMF parameters for coherent with foF2 (magenta) and all intervals analyzed (blue) Pc5/Pi3 pulsations at SOD: (a) 3-hour mean IMF B_Z; (b) 3 hour maximal dynamic pressure variation ΔP; (c) 3-hour mean SW speed V.

https://doi.org/10.5194/angeo-2020-16
Preprint. Discussion started: 13 May 2020

Annales Geophysicae Discussions
Open Access
EGU

Table 1. Coordinates and other parameters of IMAGE stations

Station	Geographic		CGM		L	MLT
	LAT	LON	Φ	Λ		midnight
SOD	67.37	26.63	64.2	106.5	5.37	21:12
MAS	69.46	23.70	66.5	105.5	6.37	21:18

Corrected geomagnetic (CGM) latitude Φ and longitude Λ, apex of the magnetic field line L, and UT of magnetic local midnight are calculated online with http://omniweb.gsfc.nasa.gov/vitmo/cgm.html

https://doi.org/10.5194/angeo-2020-16
Preprint. Discussion started: 13 May 2020

Annales Geophysicae Discussions
Open Access
EGU

Table 2. Intervals with foF2 obtained from Eq. (1) checked visually. Years 2014-2015.

Year	Month	Day	DOY	Start UT	Final UT	Comment
2014	2	24	55	9:00	14:59	
2014	4	11	101	8:00	15:59	
2014	5	24	144	7:00	15:00	Upper
2014	6	8	159	7:00	15:59	
2014	6	21	172	9:00	15:59	Upper
2014	8	18	230	8:00	15:59	
2014	9	13	256	8:00	15:59	
2014	9	14	257	8:00	15:59	
2014	9	15	258	8:00	15:59	
2014	9	16	259	8:00	15:59	
2014	9	25	268	8:00	15:59	
2014	10	15	288	8:00	15:10	
2014	10	19	292	8:00	14:30	
2014	10	24	297	8:00	12:40	
2014	10	31	304	8:00	14:59	
2014	11	6	310	8:00	14:59	
2014	11	7	311	8:00	14:59	
2014	11	8	312	8:00	13:30	
2014	11	10	314	9:00	12:30	
2014	11	11	315	9:00	14:40	
2014	11	12	316	9:00	14:59	
2014	12	7	341	9:00	12:20	
2014	12	10	344	9:00	14:59	
2014	12	13	347	9:00	14:00	
2014	12	27	361	9:00	14:20	
2014	12	29	363	9:00	12:30	
2015	1	3	3	9:00	13:20	
2015	1	22	22	9:00	12:10	
2015	1	30	30	9:00	12:20	
2015	2	15	46	9:30	13:10	
2015	3	8	67	9:00	13:40	
2015	3	10	69	9:00	15:59	
2015	3	11	70	10:50	15:00	
2015	4	4	94	9:00	14:20	
2015	5	14	134	9:00	14:20	Broad max
2015	5	15	135	9:10	15:59	Upper
2015	5	19	139	8:40	14:50	
2015	5	20	140	8:00	11:20	
2015	5	20	140	12:10	15:59	
2015	6	12	163	7:20	15:59	